

Characteristics of Amyloid-Related Oligomers Revealed by Crystal Structures of Macrocyclic β -Sheet Mimics

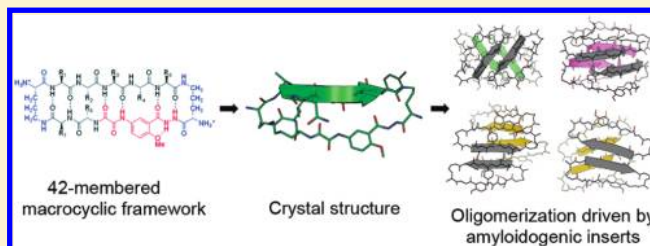
Cong Liu,^{S,†} Michael R. Sawaya,^{S,†} Pin-Nan Cheng,[‡] Jing Zheng,[‡] James S. Nowick,[‡] and David Eisenberg^{†,*}

[†]UCLA-DOE Institute for Genomics and Proteomics, Howard Hughes Medical Institute, Molecular Biology Institute, University of California, Los Angeles, California 90095, United States

[‡]Department of Chemistry, University of California, Irvine, California 92697-2025, United States

 Supporting Information

ABSTRACT: Protein amyloid oligomers have been strongly linked to amyloid diseases and can be intermediates to amyloid fibers. β -Sheets have been identified in amyloid oligomers. However, because of their transient and highly polymorphic properties, the details of their self-association remain elusive. Here we explore oligomer structure using a model system: macrocyclic peptides. Key amyloidogenic sequences from A β and tau were incorporated into macrocycles, thereby restraining them to β -strands, but limiting the growth of the oligomers so they may crystallize and cannot fibrillate. We determined the atomic structures for four such oligomers, and all four reveal tetrameric interfaces in which β -sheet dimers pair together by highly complementary, dry interfaces, analogous to steric zippers found in fibers, suggesting a common structure for amyloid oligomers and fibers. In amyloid fibers, the axes of the paired sheets are either parallel or antiparallel, whereas the oligomeric interfaces display a variety of sheet-to-sheet pairing angles, offering a structural explanation for the heterogeneity of amyloid oligomers.



INTRODUCTION

A wide range of human pathologies, including Alzheimer's disease, dialysis-related amyloidosis, and Parkinson disease, are associated with amyloid fiber formation from diverse proteins.¹ Despite the enormous variation in sequences and structures of the amyloidogenic proteins, the interaction of β -sheets is central to the assembly of soluble oligomers and mature amyloid fibers.^{2–7} Crystallographic studies have now revealed the fiberlike atomic structures of numerous amyloidogenic segments from fiber-forming proteins.⁸ The formation of parallel or antiparallel β -sheets and the assembly of pairs of β -sheets into a steric zipper are two key steps of fiber formation.⁴

Evidence has recently accumulated suggesting that, instead of amyloid fibers, soluble oligomers are the more pathogenic species in several types of protein deposition diseases.^{9–11} Studied by NMR, FTIR, EPR spectroscopy, and other methods, amyloid oligomers have been found to exhibit several common biochemical and biophysical properties: (1) amyloid oligomers contain β -sheet rich structures;^{2,3,5,6} (2) different sizes of the oligomer species coexist in solution and contribute to the heterogeneity of the oligomer mixtures;¹² (3) as an intermediate state, most of the oligomeric species are transient;¹³ (4) mediated by different protein segments, different types of oligomers can form, indicating polymorphism of amyloid oligomers,^{14–17} with some of the species showing strong structural resemblance to fibers;¹⁸ (5) oligomers formed from different amyloidogenic proteins seem to share common structural features because they are recognized by

the same antibody A11;¹⁹ (6) some of the oligomeric species show higher cytotoxicity than fibers.²⁰ Despite this knowledge, the dynamic, polymorphic, and noncrystalline behavior of the oligomeric species hinder structural studies at atomic resolution. Learning the structures of amyloid oligomers seems necessary for understanding their cellular toxicity and fiber formation, and for chemical interventions against amyloid disease.

Here we adopt macrocyclic peptides to explore the nature of amyloid oligomers. Because of the prevalence of β -sheets in biological processes such as protein–protein interactions, protein self-association, and protein aggregation, peptidic model systems which mimic β -sheets have been established.^{21–24} Nowick and co-workers recently developed macrocyclic peptides as a constrained chemical model to investigate interactions within and between β -sheets.^{25–27} The macrocyclic peptide is a 42-membered ring consisting of a pentapeptide β -strand (This is the recognition strand in Figure 1. The term “recognition” is used since it has been established that the sequence of this strand confers the ability to recognize and bind like-sequence segments in the context of larger proteins.²⁸), two δ -linked ornithines mimicking β -turns, and an antiparallel β -strand (blocking strand in Figure 1) composed of two amino acids and a “Hao” unit. The Hao unit mimics a tripeptide β -strand and is conformationally restricted to an extended β -sheet geometry by an aromatic group

Received: January 10, 2011

Published: April 07, 2011

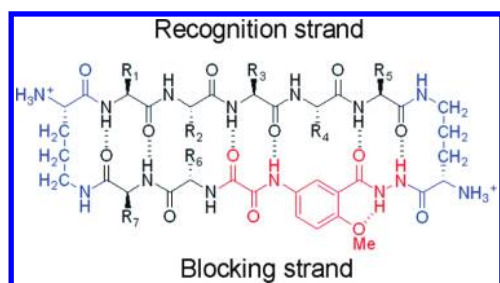


Figure 1. The 42-membered macrocyclic framework used in this study. Two δ -linked ornithine turn units are in blue. The Hao unit (red) blocks the lower edge of the recognition strand. The pentapeptide of the recognition strand (positions R1–R5) accommodates the amyloidogenic sequence of interest (Table 2). Residues in the blocking strand (positions R6 and R7) can be varied for better folding and solubility.²⁵

fused to its backbone. By forming hydrogen bonds with the recognition strand, Hao supports the β -strand conformation of the pentapeptide recognition strand. Therefore, the recognition strand is open to form edge-to-edge β -sheets with the recognition strand from a second macrocyclic peptide, whereas Hao prevents the blocking strand from further aggregation.

The 42-membered ring macrocyclic peptide mimics the β -strand conformation of polypeptides in oligomeric states. By displaying a pentapeptide sequence from the amyloidogenic polypeptide in the recognition strand, the conformation of the pentapeptide is restrained to be a β -strand, whereas the stacking of β -strands into infinite β -sheets is prevented by Hao in the blocking strand. Therefore, macrocyclic rings can freeze and homogenize the transient amyloid oligomers, and make atomic structure determination possible. Specifically, sheets would be restricted to dimers in the hydrogen bonding direction, but sheet-to-sheet interactions can expand the oligomer to tetramers.

In this work, we set out to mimic with such macrocyclic peptides the assembly and structures of amyloid oligomers associated with Alzheimer's disease. Three amyloidogenic peptides from $A\beta$ and tau known to account for the aggregation of these proteins in amyloid assemblies were displayed on macrocycles in β -strand conformation. We determined the crystal structures of these macrocycles and analyzed their structural characteristics at an atomic level. The crystal structures show that β -sheet dimers assemble into tetramers through dry, complementary interfaces between sheets. These observations, common to all four oligomeric interfaces, suggest dry, complementary interfaces are characteristic features of amyloid oligomer assembly as they are of fiber assembly. Unlike amyloid fiber structures, we observe the sheet-to-sheet pairing geometries in tetrameric oligomers to deviate from cross- β geometry by the angles of intersection of the axes of the two β -sheets of the steric zipper motifs. These variations help to explain the diversity of previously observed amyloid oligomeric polymorphs. The resulting understanding of amyloidogenic oligomer assembly at the atomic level offers clues to the design of structure-based therapeutics. In addition, macrocyclic peptides have the potential to inhibit the growth of amyloid oligomers and fibers.

EXPERIMENTAL SECTION

1. Crystallization. The four macrocyclic peptides were prepared as described previously.²⁵ The mLVF^{Br}FA, mLVFFA, mcAIFL, and mcVQIVF^{Br} were dissolved in 20 mM sodium phosphate buffer pH 7.0 containing 100 mM sodium chloride to 20, 20, 25, and 15 mg mL⁻¹,

respectively. Crystals of macrocyclic peptides were grown by mixing the peptides with an equal amount of well solution by the hanging drop vapor diffusion method. Peptide mcVQIVF^{Br} was crystallized under the condition containing Na/K phosphate pH 6.2, 35% (v/v) (\pm)-2-methyl-2,4-pentanediol, at 18 °C. The crystallization condition which gave crystals of peptide mLVF^{Br}FA contains 0.1 M sodium acetate pH 4.6, 0.17 mM calcium chloride dehydrate, 20% (v/v) 2-propanol. Crystals of peptide mLVFFA were obtained in 0.1 M MES pH 6.0, 200 mM Li₂SO₄, 20% (v/v) 1,4-butanediol. Crystals of peptide mcAIFL were obtained in 0.1 M MES pH 6.2, 0.15 mM Zn(OAc)₂, 12.5% (w/v) PEG 8000. Crystals of all four macrocyclic peptides were soaked in the cryoprotectant buffer containing the reservoir solution plus 20% (v/v) glycerol. Crystals were frozen in loops in liquid nitrogen before data collection.

2. Data Collection. X-ray diffraction data of peptide mcVQIVF^{Br} were collected at 100 K with a Rigaku FR-D X-ray generator equipped with an Raxis4++ imaging plate detector. Data of peptides mcAIFL, mLVF^{Br}FA, and mLVFFA were collected at 100 K at beamline 24-ID-C, Advanced Photon Source, Argonne National Laboratory. Denzo and XSCALE²⁹ were used for data integration and scaling. Statistics of data collection are listed in Table 1.

3. Structure Determination and Refinement. The crystal structure of mcVQIVF^{Br} was determined to 2.0 Å resolution using phases determined from a single anomalous dispersion (SAD) data set. One bromine site was located using SHELXD,³⁰ and phases were calculated with SHELXE.³¹ Model building was performed with Coot³² and illustrated with PyMOL from Delano Scientific. Crystallographic refinement was performed with the program REFMAC.³³ The model was finally refined with a TLS model using REFMAC to $R_{\text{work}} = 17.9\%$, and $R_{\text{free}} = 20.3\%$. Coordinates have been deposited with PDB accession code 3Q9G.

The crystal structure of mcAIFL was determined to 2.55 Å resolution using phases determined from a two-wavelength anomalous dispersion data set. Three zinc sites were located in space group $P6_422$ using SHELXD, and phases were calculated with SHELXE. Model building was performed with Coot and illustrated with PyMOL. Examination of side-chain packing patterns indicated the crystallographic 2-fold axes parallel and perpendicular to the 6₄ screw axis were broken, so the space group symmetry was expanded to $P3_1$. Crystallographic refinement was performed with programs REFMAC and BUSTER-TNT.³⁴ The model was finally refined to $R_{\text{work}} = 17.6\%$, and $R_{\text{free}} = 22.3\%$. Coordinates have been deposited with PDB accession code 3Q9J.

The crystal structure of mLVF^{Br}FA was determined to 2.0 Å resolution using phases determined from a single-wavelength anomalous dispersion data set. Eight bromine sites were located in space group $P4_32_12$ using SHELXD, and phases were calculated with SHELXE. Model building was performed with Coot and illustrated with PyMOL. Crystallographic refinement was performed with program REFMAC. The model was finally refined to $R_{\text{work}} = 19.6\%$, and $R_{\text{free}} = 21.8\%$. Coordinates have been deposited with PDB accession code 3Q9I. The native mLVFFA crystal was isomorphous with the bromo derivative. Phases were obtained by difference Fourier methods. The model was refined with REFMAC, then Buster/TNT to $R_{\text{work}} = 20.5$, $R_{\text{free}} = 22.2\%$. Coordinates have been deposited with PDB accession code 3Q9H.

4. Oligomer Modeling. Models of extended oligomers were built from crystal structures of the tetrameric oligomers by repeated application of 9.6 Å translations in the hydrogen-bonding direction. The models were energy minimized using conjugate gradient and simulated annealing algorithms available with the program CNS³⁵ with hydrogen bonding restraints.³⁶

RESULTS

1. Macrocyclic Peptide Design. The abnormal aggregation of $A\beta$ into amyloid plaques and tau into paired helical filaments (PHFs) are the hallmarks of Alzheimer's disease and related

Table 1. Statistics of Crystallographic Data Collection and Atomic Refinement for the Reported Four Structures

macrocycle	mcVQIVF ^{Br}	mcAIIFL	mcLVF ^{Br} FA	mcLVFFA
	Data Collection			
space group	<i>I</i> ₄ 22	<i>P</i> ₃ ₁ refinement	<i>P</i> ₆ ₄ 22 peak	<i>P</i> ₆ 22 remote
			<i>P</i> ₄ ₃ 2 ₁ 2 refinement	<i>P</i> ₄ ₃ 2 ₁ 2 phasing
				<i>P</i> ₄ ₃ 2 ₁ 2
	Cell Dimensions			
<i>a</i> , <i>b</i> , <i>c</i> (Å)	32.9, 32.9, 55.4	41.8, 41.8, 63.1	41.8, 41.8, 63.1	41.5, 41.5, 62.6
α , β , γ (deg)	90.0, 90.0, 90.0	90.0, 90.0, 120.0	90.0, 90.0, 120.0	90.0, 90.0, 120.0
wavelength (Å)	1.5418	0.9197	0.9197	0.9197
molecules per asymmetric unit	1	8	2	2
resolution (Å)	20–2.01 (2.05–2.10)	18–2.55 (2.62–2.55)	20–2.6 (2.72–2.60)	90–2.8 (2.95–2.80)
<i>R</i> _{merge} (%)	5.0 (10.9)	3.9 (50.9)	4.6 (58.7)	8.4 (50.4)
<i>I</i> / σ <i>I</i>	42.1 (22.9)	15.6 (1.7)	29.5 (3.7)	16.1 (4.2)
completeness (%)	98.2 (97.1)	98.1 (100.0)	98.8 (100.0)	99.5 (100.0)
redundancy	12.0 (12.2)	2.2 (2.3)	8.6 (8.8)	8.0 (8.2)
				13.6 (14.0)
				4.4 (4.2)
				3.3 (3.4)
	Refinement			
resolution (Å)	2.05	2.55		1.99
no. reflns	1007	3980		15 269
<i>R</i> _{work} / <i>R</i> _{free} (%)	17.9/20.3	17.8/22.4		19.6/21.8
				2.25
				10 451
				20.5/22.2
	Number of Atoms			
macrocycle	93	816 (includes alternate conformations)		744
ligand/ion	glycerol (6), acetate acid (1)	glycerol (18), zinc (8)		glycerol (18), chloride (7), isopropanol (8)
water	14	19		48
				31
	B-Factors (Å ²)			
peptide	13.5	74.0		26.8
water	27.1	73.8		40.7
				41.5
				45.8
	Root-Mean-Square Deviations			
bond lengths (Å)	0.017	0.010		0.016
bond angles (deg)	1.3	1.2		1.2
				1.3

tauopathies.^{37–39} Oligomers formed by $A\beta$ have been claimed to be the causative agents of Alzheimer's disease.⁴⁰ Even in the absence of $A\beta$, tau oligomers can cause memory impairment and neurodegeneration.⁴¹ On the basis of the participation of $A\beta$ and tau in neurodegenerative disease, key amyloidogenic segments from $A\beta$ and tau were selected and incorporated into macrocycles for structural study.

In tau oligomerization and fibrillation, segment ³⁰⁶VQIVYK³¹¹ located at the third microtubule-binding domain was revealed to be essential in mediating molecular assembly.⁴² It has the highest predicted β -sheet potential and shows a high tendency to self-associate.⁶ Proline-scanning mutations show that conformational changes in this segment from random coil to β -strand drive tau molecular assembly and aggregation.⁴² Because of the importance of ³⁰⁶VQIVYK³¹¹ in tau aggregation, the pentapeptide VQIVY was incorporated into the macrocyclic peptide mcVQIVF^{Br} (Table 2). The tyrosine hydroxyl group was replaced by a bromine atom so that crystallographic phases could be obtained by anomalous scattering methods.

Solid-state NMR studies on $A\beta$ fibers have revealed a U-shaped structure: two β -strand segments (residues 10–24 and 30–40) joined by a U-turn.^{43,44} These two segments were also observed to adopt β -strand conformations in various soluble oligomeric species and in a monomeric state stabilized by a binding partner.^{2,5,45} An observed shift from random coil to β -strand triggers the assembly of $A\beta$ molecules.² We inserted $A\beta$ residues 17–21, LVFFA, from the first amyloidogenic segment into the recognition

strand of the macrocyclic peptide mcLVFFA. In order to obtain the crystallographic phases for structure determination, we also prepared mcLVF^{Br}FA, in which the phenylalanine at position R3 is replaced by 4-bromo-phenylalanine (F^{Br}). To mimic the second amyloidogenic segment, we prepared the macrocyclic peptide mcAIIFL, a derivative of $A\beta$ residues 30–34, AIIGL, substituting Gly with Phe. This replacement improved the entire folding of the macrocycle and made it possible for crystallization and structure determination.²⁶

2. Structures of the Monomeric Macrocyclic Peptides. Extensive solution-phase studies on 42-membered macrocyclic peptides have indicated that the recognition strands tend to adopt a β -strand conformation in solution.²⁵ Here we present the first crystal structures of macrocyclic peptides in this family. Statistics for crystallographic data collection and structure refinement of macrocyclic peptides mcLVFFA, mcAIIFL, and mcVQIVF^{Br} are listed in Table 1. Figure 2a shows the crystal structures of the monomeric macrocycles. As designed, each macrocycle displays a pair of hydrogen-bonded β -strands locked into an antiparallel topology by two peptidomimetic δ -linked ornithine residues. Despite the diverse peptide sequences in the three macrocycles, the rmsd values for backbone atoms between any pair of the three structures do not exceed 1.3 Å (Table S2). The ability to accommodate a variety of sequences indicates the stability of the conserved framework (Figure S2a).

The designed incorporation of the Hao residue in the blocking strand also appears to be effective in promoting oligomeric β -sheet assembly while blocking run-away fiber formation. In

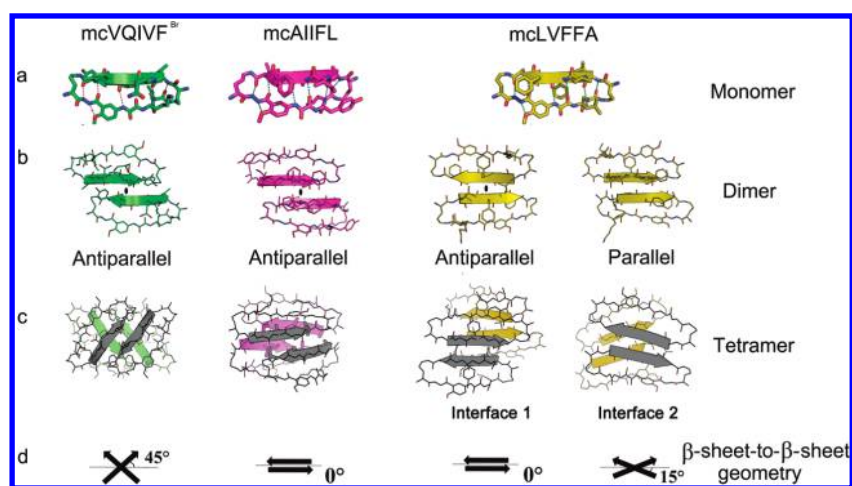


Figure 2. Crystal structures of macrocyclic peptides mcVQIVF^{Br}, mcAIIIFL, and mcLVFFA. Within the (a) monomeric structures, hydrogen bonds link the blocking and recognition strands and are shown as dotted lines. β -Sheet formation by dimeric assemblies are either parallel or antiparallel as shown in part b. (c) Molecular packing of four different tetramers. The tetrameric macrocyclic molecules form a variety of β -sheet-to- β -sheet packing geometries, deviating by 0° to 45° from cross- β geometry as shown in part d.

all three structures, the Hao residue in the blocking strand acts as an essential building block constraining the recognition strand to an extended β -strand conformation by a network of backbone hydrogen bonds with the blocking strand's Hao, R6, and R7 residues. The constrained conformation of the recognition strand facilitates formation of an intermolecular β -sheet with other β -strand molecules at its exposed edge. However, the exposed edge of the blocking strand is prohibited from interacting with other β -strand molecules by the aromatic ring and an intramolecular hydrogen bond in the Hao residue. Indeed, hydrogen-bonded self-association of macrocycles is observed in our crystal structures only in the β -sheet formed between recognition strands containing the amyloidogenic segment. This designed feature makes the macrocycle system suitable for study of the interaction patterns of amyloidogenic segments in the context of oligomers.

In addition to these designed features, an unexpected feature, a bend, was observed in the blocking strands of mcVQIVF^{Br}, mcLVFFA, and mcAIIIFL (Figure S2b). Because the bend is located at the same residue in each macrocycle (at the α -carbon of R6), a likely explanation is that it arises from an interruption of the natural pleat of the β -sheet by the Hao residue. The natural pleat of β -sheets arises from the 109° bond angle of sp³ hybridized α -carbons that connect the 3.3 Å long planar peptide linkages. The α -carbon of each successive amino acid creates a pleat opposite in direction and equal in depth to the preceding amino acid (the zigzag pattern is obvious when a sheet is viewed down the hydrogen bonding direction). The alternating directions of the pleats with equal depth give the sheet an overall flat geometry. However, in the macrocycle, the pleats are not all of equal depth. The Hao residue enforces planarity over the distance of three amino acids (about 12 Å), so the depth of the pleats (distance between tetrahedral α -carbons) varies within the blocking strand: 12 Å on the N-terminal side of R6 (where the Hao moiety is located) and 3.3 Å on the C-terminal side (where the standard peptide is located). Because the pleats are of unequal depth in the blocking strand, the appearance of an overall bent topology is conferred where the natural peptide joins the Hao plane at R6 (Figure S2b). The bend is propagated to the recognition strand (at the α -carbon of R2) by the hydrogen bonds that link it to the blocking strand. However, the bend in

Table 2. Sequences of the Macrocyclic Peptides^a

macrocyclic	amyloid sequence	R1	R2	R3	R4	R5	R6	R7
mcLVFFA	A β _{17–21}	Leu	Val	Phe	Phe	Ala	Leu	Lys
mcLVF ^{Br} FA	A β _{17–21} F19F ^{Br}	Leu	Val	Phe(Br)	Phe	Ala	Leu	Lys
mcAIIIFL	A β _{30–34} G33F	Ala	Ile	Ile	Phe	Leu	Tyr	Lys
mcVQIVF ^{Br}	Tau _{306–310} Y310F ^{Br}	Val	Gln	Ile	Val	Phe(Br)	Lys	Leu

^a Column 1 gives the abbreviation used in the text. Column 2 gives the protein from which an amyloidogenic segment between the numbered positions has been selected. Columns 3–7 give the residues inserted into the framework shown in Figure 1.

the recognition strand is less pronounced than the blocking strand. The degree of curvature is well within the range observed in natural β -sheets (Figure S2c), especially in those with fewer strands.⁴⁶

Previous studies have revealed that macrocycle solubility and folding are influenced by the choice of residues incorporated at the R6 and R7 positions;²⁵ our crystal structures offer some explanation. As might be expected, macrocycle solubility improves by incorporating a charged residue such as lysine at R6 or R7, as has been done in all three macrocycles presented here (Table 2). In all three structures, the lysine side chain extends into bulk solvent, improving the macrocycle interaction with solvent. Less obvious is the effect of the R6 and R7 side chains on folding. The interactions between the neighboring strands are limited to backbone hydrogen bonding (Figure 2a) as is typical in conventional β -sheets. The R6 and R7 side chains of the blocking strand have no van der Waals contacts with R2 and R1 of the recognition strand. In this respect, macrocycle folding should be relatively insensitive to the specific residues at R6 or R7. The reported improvement in macrocycle folding with the incorporation of an aromatic residue at R6 compared to Leu and Ala²⁵ might be attributed to a van der Waals contact between the R6 aromatic ring and the nearby ornithine hairpin turn (Figure 2a mcAIIIFL, R6 = Phe^{Br}). Such stabilization is not possible with Leu or Ala side chains because they are too short to form a contact with the ornithine turn.

3. Assembly of Dimers through β -Sheet Hydrogen-Bonding Interactions. In all three crystal structures, the macrocycles assemble into dimers via standard backbone hydrogen bonds

between recognition β -strands, forming intermolecular β -sheets (Figure 2b). One particular pattern of hydrogen bonding predominates: a 2-fold symmetric antiparallel arrangement of strands where the symmetry axis (marked by ellipses in Figure 2b) is normal to the plane of the sheet. The position of the 2-fold differs among the three structures and alters the registration between recognition strands. In mLVFFA, the 2-fold operator passes between R3 residues, whereas in mcVQIVF^{Br} and mAIIFL the 2-fold operator passes between R4 residues (Figure 2b) leaving some backbone amides at the N-termini solvent exposed. In these arrangements, the intermolecular sheet has a sidedness; the side-chains displayed on the face have different identities than those on the back. An additional parallel, out-of-register sheet is observed in the mLVFFA crystal structure (Figure 2b); the topology of the macrocyclic framework precludes homodimeric parallel in-register sheets.⁴⁷

Other types of intermolecular hydrogen-bonded arrangements are possible, but not observed. For example, one can imagine a different type of antiparallel arrangement in which the face and back of the sheets are related by 2-fold symmetry. The particular hydrogen-bonding geometry adopted by a pair of macrocycles is specified by the sequence of the recognition strand (the amyloidogenic insert). That is, the identity of side chains that come in contact across the dimer interface, their complementarity in shape and physical properties, depends on the geometry of the dimer. Side-chain packing interactions are also observed between pairs of dimers as described below, and likely play a role in specifying hydrogen-bonding geometry.

Lastly, it should be noted that there are some hydrogen-bonded arrangements which are common among globular and fibrillar proteins, but cannot be formed by macrocycle homodimers. These include parallel in-register dimers and some antiparallel pairing arrangements. Whereas the recognition strand has two nonequivalent hydrogen bonding edges, only one edge is available to form the dimer interface (formed by backbone N and O of R2 and R4); the other edge is hydrogen-bonded to the blocking strand (formed by backbone N and O of R1, R3, and R5). Hydrogen bonding with the blocking strand prohibits the two edges from interchanging. Thus, antiparallel sheet formation is limited to dimer interfaces involving backbone atoms of even numbered residues.

4. Assembly of Tetramers through Complementary Side-Chain Interactions. In all three macrocycles studied here, dimers assemble into tetramers through the interdigitation of side-chains protruding from the surfaces of the dimeric β -sheets (Figure 2c). The different tetrameric interfaces formed by the three macrocycles in crystal structures are listed in Table S3. Four of these interfaces (including two in the mLVFFA crystal) are large, burying surface areas ranging from 894 to 1089 Å² (Table S1), and mainly formed by inserted amyloidogenic segments. Their shape complementarities (0.60–0.77; Table S1) are comparable to those observed in steric zippers (0.57–0.92)⁴⁴ (Figure S3) and typical oligomeric interfaces between globular proteins (from 0.70 to 0.74).⁴⁸ The side-chains in all four interfaces are mainly hydrophobic (both aromatic and aliphatic), exclude water, and create a stable nucleation site in the tetramer. The majority of these dry interfaces are packed face-to-face (approximate D_2 symmetry), using side-chains from positions R1, R3, and R5. For example, the nucleation site of mcVQIVF^{Br} is formed mainly by π – π stacking between two pairs of Tyr side chains at the R5 positions (Figure 3a) and is supported by hydrophobic contacts between pairs of Ile side chains at position

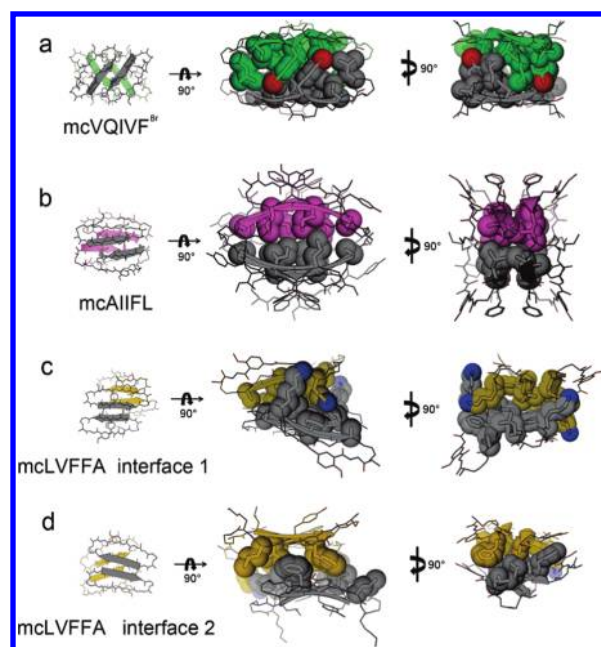


Figure 3. Side-chain interactions of the amyloidogenic segments in the macrocyclic tetramers. The designed amyloidogenic segments mediate tight and highly complementary hydrophobic interactions between macrocycle molecules. The side-chains of the segments are shown as sticks and spheres.

R3. In mAIIFL, the hydrophobic nucleation site is formed by alanine, isoleucine, and leucine side-chains at positions R1, R3, and R5 (Figure 3b). Note that the lack of participation of R4 in this tetramer interface alleviates concern about the biological relevance raised by the mutation of R4 from Gly in A β _{30–34} to Phe. In mLVFFA there are two types of interfaces. In the first, the hydrophobic nucleation site is formed by leucine, phenylalanine, and alanine side chains at positions R1, R3, and R5 (Figure 3c). However, the second interface lacks symmetry (an interface between a parallel and an antiparallel dimer), so different strands contribute different side-chains (Figure 3d). Three of the strands contribute side-chains at positions R2 and R4, while one of the strands from the parallel sheet contributes side-chains at positions R1, R3, and R5. Although residues in the blocking strand also have some contribution to the dry interface, the majority of the interface derives from the amyloidogenic insert in the recognition strand (Table S1). The predominant role played by the amyloidogenic insert suggests that the dry interfaces observed here present a very likely possibility for amyloidogenic oligomer assembly at the atomic level and may even be representative of the oligomeric packing patterns in solution. Furthermore, the tight oligomeric packing of these inserts illustrates that these segments have a strong intrinsic tendency of self-association, which is in agreement with previous studies.^{5,42,45}

Another key feature of the oligomeric interface is the variety of β -sheet-to- β -sheet packing geometries observed. In all four interfaces, the pairs of sheets interact through their flat surfaces (Figure 3). The recognition strands of the monomers can assemble as antiparallel (mLVFFA, mAIIFL, and mcVQIVF^{Br}) or parallel (mLVFFA) (Figure 2b). Variations in dimer interfaces lead to variations in tetramer interfaces; interfaces were observed between pairs of antiparallel sheets (mLVFFA interface 1, mAIIFL, and mcVQIVF^{Br}) and between a parallel and antiparallel sheet (mLVFFA interface 2). Further variations in

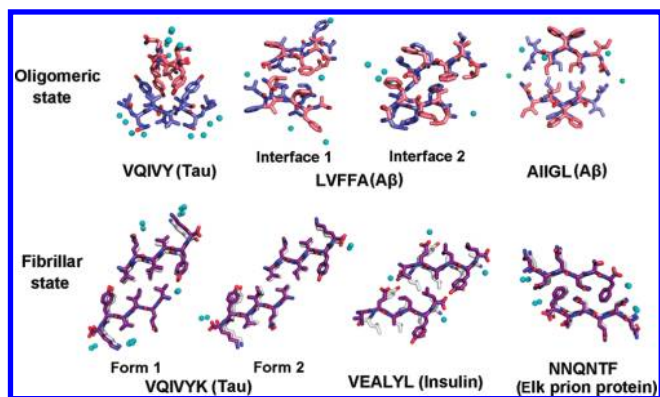


Figure 4. Comparison of the packing of amyloidogenic segments in oligomeric states (this paper) and in fibrillar states (PDB codes: 2ON9, 3FQP, 2OMQ, 3FVA). In the structures of both oligomeric states and fibrillar states, water molecules are entirely excluded from the interfaces. Amyloidogenic segments are assembled through a highly complementary, dry interface between pairs of β -sheets. The difference in packing between these two states is that in the oligomeric state, the orientation between opposing β -sheets ranges from orthogonal to parallel, whereas in the fibrillar state, the strands are constrained to either parallel or antiparallel orientations (cross- β). Water is shown in cyan spheres, and zinc is in green cyan spheres. For AIIGL from A β , Gly is replaced with Phe in the macrocycle. Phe adopts two conformations in the crystal structure and does not contribute to the tetramer packing.

tetramer interfaces involve differences in orientation between the faces of opposed β -sheets (Figure 2c); the crossing angle between β -strands of opposing sheets can be orthogonal (mcVQIVF^{Br}), antiparallel (mcAIIIFL and mcLVFFA interface 1), or somewhere in-between (mcLVFFA interface 2) (Table S1; Figure 2d).

5. Structural Features That Distinguish Amyloid-like Oligomers from Fibers. A close structural relationship exists between our tetrameric amyloid-like oligomers and fibers. The formation of a dry, highly complementary interface between pairs of β -sheets is not only a characteristic feature of these amyloid oligomers, but of amyloid fibers as well. Recently, numerous crystal structures have been reported for various amyloidogenic peptides in the fibrillar form.^{4,49} The steric zipper motif was observed in all these fiber structures. A typical steric zipper is formed by a pair of interdigitated β -sheets with no water in the interface. Figure 4 compares various amyloidogenic segments in oligomeric and fibrillar states. The structures in both states share two features: (1) architecture (the segments form β -strands, β -strands stack to β -sheets, and β -sheets pair with one another via side chains); (2) dry interface (the interactions between β -sheet layers are all dry interfaces with high shape complementarity). The area buried and shape complementarity have similar values for both oligomeric and fibrillar structures (Figure S3; Table S4). These two shared characteristics suggest that both oligomerization and fibrillation are driven by the formation of highly complementary, dry interfaces. The common observation of dry, complementary interfaces in both oligomers and fibers demonstrates the structural similarity of the two states, which is indicated also by NMR and FTIR spectrometry and conformation-dependent antibodies.^{3,14,16,18}

The primary structural difference between our macrocyclic oligomers and peptide fibers appears to be an additional degree of freedom in sheet-to-sheet packing observed in the oligomers. In the fibrillar state, the strands in opposing sheets are constrained to either parallel or antiparallel orientations (definition

of cross- β architecture).⁴ However, in the oligomeric state, the orientation between opposing β -sheets ranges from orthogonal to parallel (Figure 2c,d). Notably, the orientations between strands of opposing sheets observed in mcVQIVY (90°) and mcLVFFA (30°) are similar to values commonly reported for β -sandwiches in small globular proteins and first noted in the earlier years of protein crystallography.^{50,51} Orientations of 0° or 180° (as in mcAIIIFL and amyloid fibers) were not observed until structures with significantly larger sheets, such as GNNQQNY⁸ and β -helix proteins,⁵² were revealed. Indeed, it seems likely that the greater geometric constraints imposed in the fibers compared to oligomers arise from the larger number of molecules in each β -sheet; there might be thousands of β -strands in a sheet within a fiber, but only a few dozen in an oligomer. Consequently, there are additional degrees of freedom in the side-chain rotamers of oligomers compared to fibers. The additional degrees of freedom can accommodate additional (non-cross- β) sheet-to-sheet packing geometries. In short, the most pronounced difference in the geometries of some of these amyloid oligomers from amyloid fibers is the deviation of the axes of the interacting sheets of the oligomers from 0° or 180°.

DISCUSSION

A variety of morphologies have been described for amyloidogenic oligomers. Considering A β alone, nine types of oligomers have been identified including prefibrillar oligomers, fibrillar oligomers, annular protofibrils, and others.^{2,12,15,16,18} Molecular weights of these oligomers range from 10 kDa dimers to 700 kDa amylospheroids. Models proposed for these β -rich solution oligomers can be roughly divided into two groups depending on the way the β -sheets self-assemble. In one group, the β -sheets wrap around to form a topologically closed cylinder or β -barrel so that all main chain hydrogen bond donors and acceptors of the β -strands are satisfied. Models of β -barrels include an antiparallel single β -sheet cylinder³ and a parallel double layer β -barrel.⁵³ In the other group the β -sheets are open, leaving exposed main chain hydrogen bond donors and acceptors on the β -sheet edges. Models of open sheet oligomers include one constructed from a U-shaped building block,⁵⁴ and one constructed from a β -hairpin building block.^{45,55,56}

Our atomic oligomer models more closely resemble the second group: open sheet oligomers. Indeed, a cylindrical topology is prohibited by the blocking strand used in the macrocyclic design. We propose that the tetrameric oligomers of the type described here could exist in solution in the absence of the blocking strand. Since these tetramers are smaller than most reported oligomers of A β , it is tempting to speculate that the tetramers could be building blocks for larger molecular weight oligomers. In the absence of a blocking strand, expansion of the oligomer size is most likely to occur through addition of β -strands at the exposed edges of the β -sheets. Growth of the oligomer is likely to stop more quickly if the crossing angle between the two sheets is large, since the addition of strands would not increase the size of the dry interface, and the growing single sheets would be solvent exposed and labile. However, if the axes of the two sheets are nearly parallel, that is, closer to cross- β geometry, the addition of each strand would proportionally increase the area of the dry interface, providing the driving force that could lead to the formation of amyloid fibers (Figure 5).

The particular sheet-to-sheet packing adopted by an oligomer may distinguish it as being either on-pathway or off-pathway to

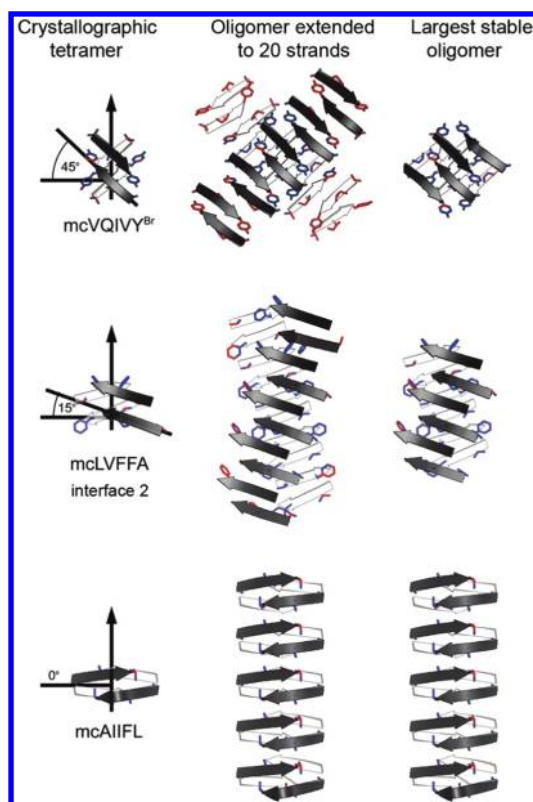


Figure 5. Models of extended amyloid-like oligomers (right column), extrapolated from crystallographic tetramers (left column). Extended oligomers were modeled by continuing the hydrogen-bonding pattern in the tetramer with the addition of β -strands at the exposed edges of the tetramer until a 20mer is achieved (middle column). Side-chains are shown for those residues that face the opposing sheet. The side-chain atoms are colored red if they are solvent exposed and blue if they are buried by the opposing sheet. The maximum stable size of the oligomer was estimated by removing those strands in which over 50% of the side-chain atoms are exposed (right column).

fiber formation. Only the oligomeric species with approximate cross- β geometry can further associate into higher oligomers and eventually form fibers. Other oligomers may be trapped in various off-pathway oligomeric species (Figure 5). Some of these oligomers are toxic with characteristically high β -sheet content.^{2,10,14–16,18} One might imagine that if cell toxicity requires the β -sheet aggregate to have a particular structure, an oligomer might be able to achieve that structure more readily than a fiber, because oligomers can sample more conformations than fibers. This might explain the phenomenon that some amyloid oligomeric species are pathogenic or more toxic than the fibers.

Our structures help to explain the great polymorphism of amyloid oligomers. The observed variation in oligomeric geometry among the three macrocycles presumably arises from differences in the sequence of the amyloidogenic insert, but also polymorphic variations occur within the same crystal (compare mcLVFFA interfaces 1 and 2, Figure 3c,d). The polymorphism observed with the mcLVFFA crystal suggests that polymorphism observed in $A\beta$ and other amyloid oligomers may result in part from analogous differences in hydrogen bonding patterns and sheet-to-sheet packing geometries. Furthermore, many amyloidogenic proteins have more than one amyloidogenic segment and may encounter different environments during molecular assembly.⁴⁹ The local environment may influence the type of

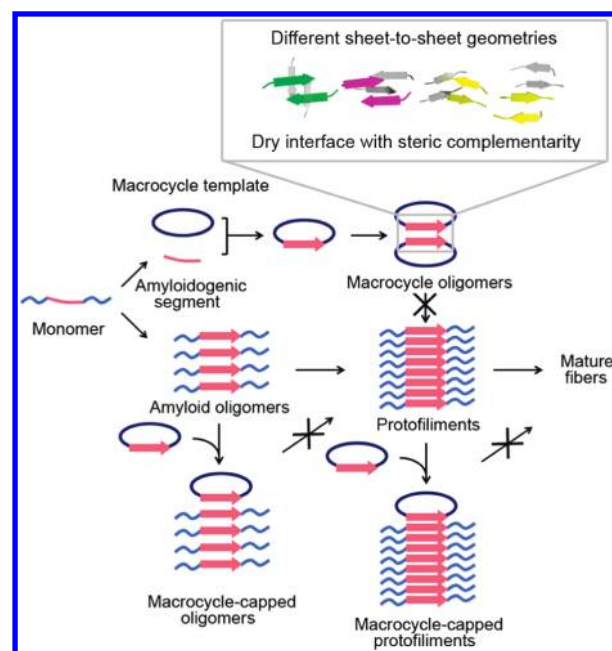


Figure 6. Schematic diagram of macrocyclic peptides mimicking amyloidogenic protein self-assembly. Amyloid proteins are shown in light blue with amyloidogenic segments in pink. Mediated by amyloidogenic segments, an amyloidogenic protein forms transient and highly polymorphic oligomers, protofilaments, and eventually mature fibers. By displaying the amyloidogenic peptides in the recognition strand of a macrocycle as a β -strand, the conformation of the peptides during self-assembly is mimicked. The Hao residue in the macrocyclic ring blocks the infinite molecular assembly and captures a single oligomeric state for X-ray crystallographic studies. The structures of the macrocycles reflect one very likely possibility for amyloid oligomer assembly. By mixing a macrocycle with an amyloidogenic protein, the β -strand mimics can interact with the same segment in the native protein. The Hao residue as a blocker may stop oligomers from further association into fibers and also cap protofilaments from elongation and maturation by binding at the growing edge of the sheets.

interface formed during self-assembly. Thus, under different conditions, different segments, or different residues in the same segment may be involved in different types of oligomer formation. Therefore, the number of different potential interactions may account for one of the most distinct features of amyloid oligomers: polymorphism.

Despite the diversity of oligomer assembly, our crystal structures also show that soluble proteins with entirely different sequences fold into the β -sheet-rich structures with the common dry steric complementary interfaces. Polyphenols and small aromatic peptides such as (–)-epigallocatechin gallate (EGCG) and resveratrol which were shown to disrupt the amyloid oligomers and fibers formed by different proteins^{57–60} may target the dry interface. By disrupting the dry interface, polyphenols may dissolve amyloid oligomers, incorporate into the amyloidogenic polypeptides, and form off-pathway oligomers with diminished cytotoxicity and reduced strand content.^{58,59} This suggests that compounds which can disrupt the dry interface of the amyloid oligomers could be potential drug candidates for broad-spectrum therapeutic treatments against amyloidogenic diseases.

In addition to facilitating structural research on amyloid oligomers, macrocycles with amyloidogenic segments inserted are potential inhibitors against amyloid oligomerization and fibrillation, as summarized in Figure 6. The amyloidogenic proteins are

intrinsically disordered. They expose their amyloidogenic segments, which can self-associate into self-complementary complexes. The initial aggregation process leads to the formation of oligomeric intermediates. By mimicking the conformation of the amyloid oligomeric state, the macrocycle with the same amyloidogenic segment inserted could interact with the exposed segment of the protein. With Hao molecules preventing further assembly, the macrocycle molecules trap the amyloidogenic protein in a low molecular weight oligomer. Furthermore, the β -sheet conformation of the amyloidogenic segments of the macrocycles is compatible with the conformation of β -strands in steric zipper structures (Figure S4). The macrocycle could bind stably to the growing end of the protofilament and prevent additional molecules from binding and elongating the fibers. Indeed, the macrocycle which contains VQIVY in the recognition strand shows strong inhibition of AcPHF6 fibrillation.²⁸

ASSOCIATED CONTENT

S Supporting Information. Complete ref 14, figures including electron density maps and superposition of the macrocyclic structures, further analysis of the amyloidogenic segments in oligomeric and fibrillar forms, overlapping the amyloidogenic segments of macrocycles with steric zipper fibril structures, and tables including sequences and structural statistics of the macrocyclic peptides. This material is available free of charge via the Internet at <http://pubs.acs.org>.

AUTHOR INFORMATION

Corresponding Author

david@mbi.ucla.edu

Author Contributions

[§]These authors contributed equally to this work.

ACKNOWLEDGMENT

We thank the NE-CAT beamline, the Advanced Photon Source for beam time and collection assistance. We thank NIH (GM-49076 and AG-029430), NSF, and HHMI for grant support.

REFERENCES

- (1) Buxbaum, J. N. *Curr. Opin. Rheumatol.* **2004**, *16*, 67–75.
- (2) Ono, K.; Condrón, M. M.; Teplow, D. B. *Proc. Natl. Acad. Sci. U.S.A.* **2009**, *106*, 14745–14750.
- (3) Cerf, E.; Sarroukh, R.; Tamamizu-Kato, S.; Breydo, L.; Derclaye, S.; Dufrene, Y. F.; Narayanaswami, V.; Goormaghtigh, E.; Ruysschaert, J. M.; Raussens, V. *Biochem. J.* **2009**, *421*, 415–423.
- (4) Sawaya, M. R.; Sambashivan, S.; Nelson, R.; Ivanova, M. I.; Sievers, S. A.; Apostol, M. I.; Thompson, M. J.; Balbirnie, M.; Wiltzius, J. J.; McFarlane, H. T.; Madsen, A. O.; Riek, C.; Eisenberg, D. *Nature* **2007**, *447*, 453–457.
- (5) Chimon, S.; Shaibat, M. A.; Jones, C. R.; Calero, D. C.; Aizezi, B.; Ishii, Y. *Nat. Struct. Mol. Biol.* **2007**, *14*, 1157–1164.
- (6) von Bergen, M.; Barghorn, S.; Biernat, J.; Mandelkow, E. M.; Mandelkow, E. *Biochim. Biophys. Acta* **2005**, *1739*, 158–166.
- (7) Makin, O. S.; Serpell, L. C. *FEBS J.* **2005**, *272*, 5950–5961.
- (8) Nelson, R.; Sawaya, M. R.; Balbirnie, M.; Madsen, A. O.; Riek, C.; Grothe, R.; Eisenberg, D. *Nature* **2005**, *435*, 773–778.
- (9) Conway, K. A.; Lee, S. J.; Rochet, J. C.; Ding, T. T.; Williamson, R. E.; Lansbury, P. T., Jr. *Proc. Natl. Acad. Sci. U.S.A.* **2000**, *97*, 571–576.
- (10) Sakono, M.; Zako, T. *FEBS J.* **2010**, *277*, 1348–1358.
- (11) Meraz-Rios, M. A.; Lira-De Leon, K. I.; Campos-Pena, V.; De Anda-Hernandez, M. A.; Mena-Lopez, R. *J. Neurochem.* **2010**, *112*, 1353–1367.
- (12) Bernstein, S. L.; Dupuis, N. F.; Lazo, N. D.; Wyttenbach, T.; Condrón, M. M.; Bitan, G.; Teplow, D. B.; Shea, J. E.; Ruotolo, B. T.; Robinson, C. V.; Bowers, M. T. *Nat. Chem.* **2009**, *1*, 326–331.
- (13) Smith, D. P.; Radford, S. E.; Ashcroft, A. E. *Proc. Natl. Acad. Sci. U.S.A.* **2010**, *107*, 6794–6798.
- (14) Yu, L. P.; et al. *Biochemistry* **2009**, *48*, 1870–1877.
- (15) Glabe, C. G. *J. Biol. Chem.* **2008**, *283*, 29639–29643.
- (16) Ahmed, M.; Davis, J.; Aucoin, D.; Sato, T.; Ahuja, S.; Aimoto, S.; Elliott, J. I.; Van Nostrand, W. E.; Smith, S. O. *Nat. Struct. Mol. Biol.* **2010**, *17*, 561–567.
- (17) Kaye, R.; Pensalfini, A.; Margol, L.; Sokolov, Y.; Sarsoza, F.; Head, E.; Hall, J.; Glabe, C. *J. Biol. Chem.* **2009**, *284*, 4230–4237.
- (18) Wu, J. W.; Breydo, L.; Isas, J. M.; Lee, J.; Kuznetsov, Y. G.; Langen, R.; Glabe, C. *J. Biol. Chem.* **2010**, *285*, 6071–6079.
- (19) Kaye, R.; Head, E.; Thompson, J. L.; McIntire, T. M.; Milton, S. C.; Cotman, C. W.; Glabe, C. G. *Science* **2003**, *300*, 486–489.
- (20) Caughey, B.; Lansbury, P. T. *Annu. Rev. Neurosci.* **2003**, *26*, 267–298.
- (21) Hughes, R. M.; Waters, M. L. *Curr. Opin. Struct. Biol.* **2006**, *16*, 514–524.
- (22) Gellman, S. H. *Curr. Opin. Chem. Biol.* **1998**, *2*, 717–725.
- (23) Nowick, J. S. *Acc. Chem. Res.* **2008**, *41*, 1319–1330.
- (24) Khakshoor, O.; Nowick, J. S. *Curr. Opin. Chem. Biol.* **2008**, *12*, 722–729.
- (25) Woods, R. J.; Brower, J. O.; Castellanos, E.; Hashemzadeh, M.; Khakshoor, O.; Russu, W. A.; Nowick, J. S. *J. Am. Chem. Soc.* **2007**, *129*, 2548–2558.
- (26) Khakshoor, O.; Demeler, B.; Nowick, J. S. *J. Am. Chem. Soc.* **2007**, *129*, 5558–5569.
- (27) Khakshoor, O.; Lin, A. J.; Korman, T. P.; Sawaya, M. R.; Tsai, S. C.; Eisenberg, D.; Nowick, J. S. *J. Am. Chem. Soc.* **2010**, *132*, 11622–11628.
- (28) Zheng, J.; Liu, C.; Sawaya, M. R.; Vadla, B.; Khan, S.; Woods, R. J.; Eisenberg, D.; Goux, W. J.; Nowick, J. S. *J. Am. Chem. Soc.* **2011**, Article ASAP, DOI: 10.1021/ja110545h
- (29) (a) Otwinowski, Z.; Minor, W. *Methods Enzymol.* **1997**, *276*, Macromolecular Crystallography, part A, 307–326. (b) Kabsch, W. *J. Appl. Crystallogr.* **1993**, *26*, 795–800.
- (30) Schneider, T. R.; Sheldrick, G. M. *Acta Crystallogr., Sect. D: Biol. Crystallogr.* **2002**, *58*, 1772–1779.
- (31) Sheldrick, G. M. *Acta Crystallogr., Sect. A: Cryst. Phys., Diffraction, Theor. Gen. Crystallogr.* **2008**, *64*, 112–122.
- (32) Emsley, P.; Cowtan, K. *Acta Crystallogr., Sect. D: Biol. Crystallogr.* **2004**, *60*, 2126–2132.
- (33) Murshudov, G. N.; Vagin, A. A.; Dodson, E. J. *Acta Crystallogr., Sect. D: Biol. Crystallogr.* **1997**, *53*, 240–255.
- (34) Bricogne, G.; Blanc, E.; Brandl, M.; Flensburg, C.; Keller, P.; Paciorek, W.; Roversi, P.; Smart, O. S.; Vonnrhein, C.; Womack, T. O. *REFMAC and BUSTER-TNT*; Global Phasing Ltd.: Cambridge, U.K., 2009.
- (35) Korostelev, A.; Bertram, R.; Chapman, M. S. *Acta Crystallogr., Sect. D: Biol. Crystallogr.* **2002**, *58*, 761–767.
- (36) Fabiola, F.; Bertram, R.; Korostelev, A.; Chapman, M. S. *Protein Sci.* **2002**, *11*, 1415–1423.
- (37) LaFerla, F. M.; Oddo, S. *Trends Mol. Med.* **2005**, *11*, 170–176.
- (38) Hardy, J. A.; Higgins, G. A. *Science* **1992**, *256*, 184–185.
- (39) Ballatore, C.; Lee, V. M.; Trojanowski, J. Q. *Nat. Rev. Neurosci.* **2007**, *8*, 663–672.
- (40) Walsh, D. M.; Selkoe, D. J. *J. Neurochem.* **2007**, *101*, 1172–1184.
- (41) Kaye, R.; Jackson, G. R. *Curr. Opin. Immunol.* **2009**, *21*, 359–363.
- (42) von Bergen, M.; Friedhoff, P.; Biernat, J.; Heberle, J.; Mandelkow, E. M.; Mandelkow, E. *Proc. Natl. Acad. Sci. U.S.A.* **2000**, *97*, 5129–5134.
- (43) Paravastu, A. K.; Leapman, R. D.; Yau, W. M.; Tycko, R. *Proc. Natl. Acad. Sci. U.S.A.* **2008**, *105*, 18349–18354.
- (44) Luhrs, T.; Ritter, C.; Adrian, M.; Riek-Loher, D.; Bohrmann, B.; Döbeli, H.; Schubert, D.; Riek, R. *Proc. Natl. Acad. Sci. U.S.A.* **2005**, *102*, 17342–17347.

- (45) Hoyer, W.; Gronwall, C.; Jonsson, A.; Stahl, S.; Hard, T. *Proc. Natl. Acad. Sci. U.S.A.* **2008**, *105*, 5099–5104.
- (46) Koh, E.; Kim, T.; Cho, H. *Bioinformatics* **2006**, *22*, 297–302.
- (47) Levin, S.; Nowick, J. S. *J. Am. Chem. Soc.* **2007**, *129*, 13043–13048.
- (48) Lawrence, M. C.; Colman, P. M. *J. Mol. Biol.* **1993**, *234*, 946–950.
- (49) Wiltzius, J. J.; Landau, M.; Nelson, R.; Sawaya, M. R.; Apostol, M. I.; Goldschmidt, L.; Soriaga, A. B.; Cascio, D.; Rajashankar, K.; Eisenberg, D. *Nat. Struct. Mol. Biol.* **2009**, *16*, 973–978.
- (50) Chothia, C.; Janin, J. *Proc. Natl. Acad. Sci. U.S.A.* **1981**, *78*, 4146–4150.
- (51) Chothia, C.; Janin, J. *Biochemistry* **1982**, *21*, 3955–3965.
- (52) Jenkins, J.; Pickersgill, R. *Prog. Biophys. Mol. Biol.* **2001**, *77*, 111–175.
- (53) Jang, H.; Zheng, J.; Nussinov, R. *Biophys. J.* **2007**, *93*, 1938–1949.
- (54) Zheng, J.; Yu, X.; Wang, J.; Yang, J. C.; Wang, Q. *J. Phys. Chem. B* **2010**, *114*, 463–470.
- (55) Sandberg, A.; Luheshi, L. M.; Sollvander, S.; Pereira de Barros, T.; Macao, B.; Knowles, T. P.; Biverstal, H.; Lendel, C.; Ekholm-Petterson, F.; Dubnovitsky, A.; Lannfelt, L.; Dobson, C. M.; Hard, T. *Proc. Natl. Acad. Sci. U.S.A.* **2010**, *107*, 15595–15600.
- (56) Strodel, B.; Lee, J. W.; Whittleston, C. S.; Wales, D. J. *J. Am. Chem. Soc.* **2010**, *132*, 13300–13312.
- (57) Scherzer-Attali, R.; Pellarin, R.; Convertino, M.; Frydman-Marom, A.; Egoz-Matia, N.; Peled, S.; Levy-Sakin, M.; Shalev, D. E.; Caffisch, A.; Gazit, E.; Segal, D. *PLoS One* **2010**, *5*, e11101.
- (58) Ehrnhoefer, D. E.; Bieschke, J.; Boeddrich, A.; Herbst, M.; Masino, L.; Lurz, R.; Engemann, S.; Pastore, A.; Wanker, E. E. *Nat. Struct. Mol. Biol.* **2008**, *15*, 558–566.
- (59) Bieschke, J.; Russ, J.; Friedrich, R. P.; Ehrnhoefer, D. E.; Wobst, H.; Neugebauer, K.; Wanker, E. E. *Proc. Natl. Acad. Sci. U.S.A.* **2010**, *107*, 7710–7715.
- (60) Ladiwala, A. R.; Lin, J. C.; Bale, S. S.; Marcelino-Cruz, A. M.; Bhattacharya, M.; Dordick, J. S.; Tessier, P. M. *J. Biol. Chem.* **2010**, *285*, 24228–24237.